PHYSICAL REVIEW B **80**, 140415(R) (2009)

Magnetoelectric coupling and electric control of magnetization in ferromagnet/ferroelectric/normal-metal superlattices

Tianyi Cai,[1,2] Sheng Ju,[3] Jaekwang Lee,[1] Na Sai,[1] Alexander A. Demkov,[1] Qian Niu,[1] Zhenya Li,[3] Junren Shi,[2] and Enge Wang[2]

[1]*Department of Physics, The University of Texas, Austin, Texas 78712, USA*

[2]*Institute of Physics and ICQS, Chinese Academy of Sciences, Beijing 100080, China*

[3]*Department of Physics and Jiangsu Key Laboratory of Thin Films, Soochow University, Suzhou 215006, China*

(Received 2 August 2009; revised manuscript received 4 October 2009; published 29 October 2009)

Ferromagnet/ferroelectric/normal-metal superlattices are proposed to realize the large room-temperature magnetoelectric effect. Spin-dependent electron screening is the fundamental mechanism at the microscopic level. We also predict an electric control of magnetization in this structure. The naturally broken inversion symmetry in our tricomponent structure introduces a magnetoelectric coupling energy of PM^2. Such a magnetoelectric coupling effect is general in ferromagnet/ferroelectric heterostructures, independent of particular chemical or physical bonding, and will play an important role in the field of multiferroics.

DOI: 10.1103/PhysRevB.80.140415 PACS number(s): 85.50.Gk

Ferroelectricity and ferromagnetism are important in many technological applications and the quest for multiferroic materials, where these two phenomena are intimately coupled, is of significant technological and fundamental interests.[1–6] In general, ferroelectricity and ferromagnetism tend to be mutually exclusive or interact weakly with each other when they coexist in a single-phase material.[2] Increasing the spin-orbit interaction of the electrons[7] or strategically designing for magnetic and electric phase controls[6,8] may enhance the magnetoelectric (ME) coupling effect in a single-phase multiferroic material. Practical applications of the ME effect, however, remain hindered by the small electric polarization and low Curie temperature.[3–5]

Artificial composites of ferroic materials may enable the room-temperature ME effect since both large and robust electric and magnetic polarizations can persist to room temperature. Two types of ME coupling at a ferromagnet (FM)/dielectric interface have been reported: one employing the mechanical interaction[9,10] or chemical bonding[11] and the other one employing mediation by carriers (screening charges).[12–15] The role of electrostatic screening in ferroelectric (FE) capacitors has been studied by macroscopic models.[16] Recently, *ab initio* studies of nanoscale FE capacitors[17,18] and FE tunnel junctions[19–21] have further confirmed that electrostatic screening is the fundamental mechanism at the FE/normal-metal (NM) interface. In this Rapid Communication we propose a strategy of achieving robust ME coupling in a tricomponent FM/FE/NM superlattice. The additional magnetization, caused by spin-dependent screening,[12,13] will accumulate at each FM/FE interface. Due to the broken inversion symmetry between the FM/FE and the NM/FE interfaces, there would be a net additional magnetization in each FM/FE/NM unit cell, unlike the symmetric structures discussed in the previous work. The addition of magnetization in this superlattice will result in a large global magnetization.

The tricomponent superlattice is illustrated in Fig. 1(a). When the FE layer is polarized, surface charges are created. These bound charges are compensated by the screening charge in both FM and NM electrodes. In the FM metal, the screening charges are spin polarized due to the ferromagnetic exchange interaction. The spin dependence of screening leads to additional magnetization in the FM electrode as illustrated in Fig. 1(b). If the density of screening charges is denoted as η and the spin polarization of screening charges is denoted as ζ, we can directly express the induced magnetization per unit area as

$$\Delta M = \frac{\eta}{e}\zeta\mu_B. \tag{1}$$

As this effect depends on the orientation of the electric polarization in FE, the ME coupling is expected.

Before starting specific calculations, let us consider two simple cases. (1) In an ideal capacitor where all the surface charges reside at the metal (FM or NM)/FE interfaces, the density of screening charge η reaches its maximum value $\eta=P_0$, where P_0 is the spontaneous polarization of the FE. This results in a large induced magnetization $[(P_0/e)\zeta\mu_B]$.

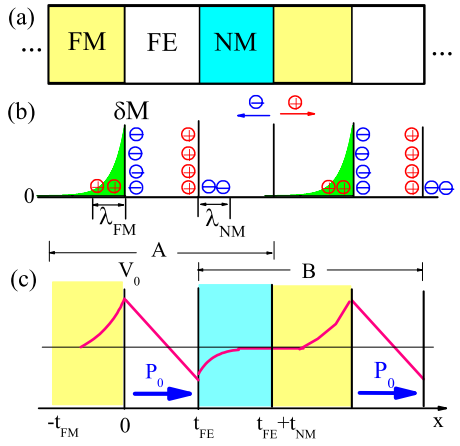

FIG. 1. (Color online) (a) Schematic illustration of FM/FE/NM tricomponent superlattice. (b) The distribution of charges and induced magnetization (green shaded area) calculated by our theoretical model. A and B are two different choices of the unit cell. The directions of arrows indicate the motions of positive and negative charges across the boundary of the unit cell A. (c) Electrostatic potential profile.

TABLE I. Parameters extracted from band structures of Ni, Co, and Fe from Ref. 12 and CrO_2 from Ref. 22. Here, ΔM is the value at $V_a = V_C$, where V_a is the applied bias and V_C is the coercive bias.

FM	J (eV nm^3)	N_0 (eV^{-1} nm^{-3})	$M_0/\mu_B N_0$ (%)	λ_{FM} (Å)	ΔM (μ_B nm^{-2})	τ (G cm/V)
Ni	0.65	1.74	−79.3	0.9	−0.280	0.015
Co	1.25	0.89	−58.4	1.5	−0.126	0.004
Fe	2.40	1.11	56.8	1.3	0.078	0.003
CrO_2	1.8	0.69	100	1.7	0.323	0.010

(2) In half metals, there is only one type of carriers that can provide the screening. If a half metal is chosen to be the FM electrode, the screening electrons will be completely spin polarized. In this case, a large induced magnetization is also expected, $\Delta M = \frac{\eta}{e}\mu_B$.

Induced magnetization from screening charges. For simplicity, we will first consider the case of zero bias, as illustrated in Fig. 1(c). Here, the following assumptions are made. (1) The difference in the work function between FM and NM is ignored. (2) To screen the bound charges in FE, the charges in metal electrodes will accumulate at the FM/FE side, and there is a depletion at the NM/FE side. In this process, the total amount of charge is conserved; however, the spin density is not conserved because of the ferromagnetic exchange interaction in the FM metal.

As shown in Fig. 1, the *local* induced magnetization, defined as $\delta M(x) = [\delta n^{\uparrow}(x) - \delta n^{\downarrow}(x)]\mu_B$, is a function of distance from the interface x. Here, $\delta n^{\sigma}(x)$ is the density of the *induced* screening charges with spin σ. Zhang[12] considered the FM/dielectric interface within the linearized Thomas-Fermi model and derived two coupled equations relating the local induced magnetization $\delta M(x)$ and the screening potential $V_0(x)$,

$$\delta M(x) = -\frac{M_0/\mu_B}{1 + JN_0} eV_0(x),$$

$$\frac{d^2V_0(x)}{dx^2} = \frac{1}{\lambda_{FM}^2} V_0(x). \tag{2}$$

The screening length in the FM electrode is defined as $\lambda_{FM} = \{(e^2N_0/\varepsilon_0)\{[N_0 + JN_0^2 - J(M_0/\mu_B)^2]/(1 + JN_0)\}\}^{-1/2}$, where $N_0 = N^{\uparrow} + N^{\downarrow}$ is the total density of states, $M_0 = (N^{\uparrow} - N^{\downarrow})\mu_B$ can be thought of as the spontaneous magnetization, ε_0 is the vacuum dielectric constant, and J is the strength of the ferromagnetic exchange coupling in the FM layer.

We solve the above equations for our unit cell and obtain

$$V_0(x) = \begin{cases} \dfrac{\eta\lambda_{FM}}{\varepsilon_0} e^{x/\lambda_{FM}}, & -t_{FM} \le x \le 0 \\ -\dfrac{\eta\lambda_{NM}}{\varepsilon_0} e^{-(x - t_{FE})/\lambda_{NM}}, & t_{FE} \le x \le t_{FE} + t_{NM}, \end{cases} \tag{3}$$

where η is the density of screening charges; $\lambda_{FM(NM)}$ is the screening length of FM (NM) electrode; and t_{FM}, t_{FE}, and t_{NM} are the thicknesses of FM, FE, and NM layers, respectively. From the above equations, we see that the local induced magnetization $\delta M(x)$ decays exponentially away from the FM/FE interface. This distribution is identical to that of screening charges, because in our model the effective interaction J in FM is assumed to be a constant. The total induced magnetization ΔM can be calculated by integrating $\delta M(x)$ over the FM layer,

$$\Delta M = \int_{FM\ \text{layer}} \delta M(x) = -\frac{\eta M_0/e}{N_0 + JN_0^2 - J(M_0/\mu_B)^2}. \tag{4}$$

The effective spin polarization of screening electrons can then be written as

$$\zeta = -\frac{M_0}{N_0 + JN_0^2 - J(M_0/\mu_B)^2}. \tag{5}$$

We have considered the induced magnetization in FM/FE/NM tricomponent superlattice with several FM electrodes, i.e., Fe, Co, Ni, and CrO_2. Detailed parameters and calculated values of ΔM are listed in Table I. The magnitude of ΔM is found to depend strongly on the choice of the FM and FE. Among the normal FM metals (Ni, Co, and Fe), the largest ΔM is observed in Ni for its smallest J and highest spontaneous spin polarization $M_0/\mu_B N_0$. On the other hand, we also predict a large ΔM for the 100% spontaneous spin polarization in half-metallic CrO_2.

To confirm the validity of our model, we perform first-principles calculations of the Fe/FE/Pt superlattice.[23] The calculations are within the local-density approximation to density-functional theory and are carried out with VASP.[24] We choose $BaTiO_3$ (BTO) and $PbTiO_3$ (PTO) for the FE layer. Starting from the ferroelectric $P4mm$ phase of BTO and PTO with polarization pointing along the superlattice stacking direction, we perform a structural optimization of the multilayer structures by minimizing their total energies. The in-plane lattice constants are fixed to those of the tetragonal phase of bulk FEs. Figure 2 shows the calculated induced magnetic moment relative to that of bulk Fe near the Fe/BTO interface when the polarization in $BaTiO_3$ points toward the Fe/BTO interface. It is evident that the induced moments decay exponentially as the distance from the interface increases. This result is in line with our model for the magnetization accumulation in the FM at the FM/FE interface. A numerical fitting of the exponential function yields a screening length of ~0.7 Å for the Fe/$BaTiO_3$/Pt structure. This value is comparable to the screening length parameters calculated using the theoretical model as shown in Table I.

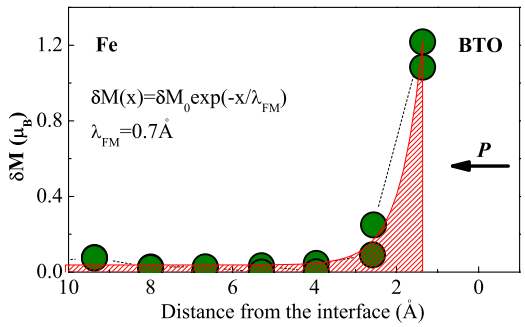

FIG. 2. (Color online) Layer-resolved induced magnetic moment of Fe near the interface between Fe and $BaTiO_3$ in the $Fe/BaTiO_3/Pt$ superlattice. Solid line is the fitted exponential function for the induced moment as a function of the distance from the interface.

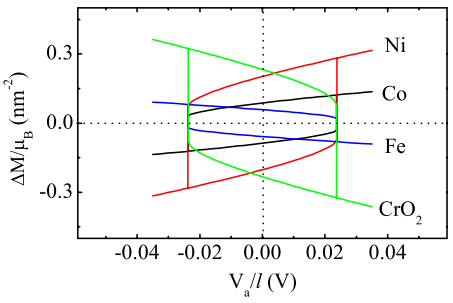

FIG. 3. (Color online) ΔM versus V_a/l for different ferromagnetic metal electrodes. V_a is the applied bias and l is the number of the unit cell. Here, the thickness of FE layer is 3 nm. However, a thicker FE layer can be used to avoid the possible electron tunneling effect.

Using our theoretical model we also calculate the ME coupling coefficient τ, which is defined as the ratio of the magnetization change $2\mu_0\Delta M/\lambda_{FM}$ to the coercive field $V_C/(lt_{FE})$, where V_C is the coercive voltage and l is the number of the unit cell. The τ values listed in Table I reach as large as 0.015 G cm/V in Ni. For comparison, τ of about 0.01 G cm/V arising from the chemical bonding between Fe and Ti atoms is predicted for the $Fe/BaTiO_3$ bilayer.[11] The ME coefficient measured in epitaxial $BiFeO_3$-$CoFe_2O_4$ columnar nanostructures[10] is also 0.01 G cm/V. We should point out that in our calculation the coercive field is assumed to be 200 kV/cm; if we choose the coercive field of 10 kV/cm same as Ref. 11, τ will be 20 times larger than those listed in Table I. Therefore, the ME effect arising from spin-dependent electron screening in FM/FE/NM tricomponent superlattice can be *much larger* than in other composite multiferroics.

What is the source of this large ME effect? In fact, the magnetoelectric effect discussed in this Rapid Communication is not the usual bulk magnetoelectric coupling at all. Spontaneous electric polarization in FE results in the induced surface charge. In turn, this produces the screening charges of density η. These screening charges are polarized with the polarization ζ. Therefore, it is the amount of screening charges and polarization that determine the magnitude of the ME effect (ΔM and τ). If we expand the induced magnetization ΔM in Eq. (4) as a power series in order parameters P_0 and M_0 (spontaneous polarization and magnetization), we obtain

$$\Delta M \propto P_0 M_0 + \text{high-order terms in } P_0 \text{ and } M_0. \quad (6)$$

The higher-order terms in Eq. (3) vanish exactly in the following limiting case: the screening length $\lambda_{FM} \to 0$ and spin polarization $\zeta \to \pm 100\%$. In general, the leading term in Eq. (6) is linear, which is consistent with the computational result of Ref. 13. It is also clear that this effect depends on the magnetization of the ferromagnetic metal.

First-principles calculations confirm the central conclusion that the ME coupling in the tricomponent system is linear in polarization of FE. We compare a superlattice with BTO and that with PTO. The induced magnetization difference is 3.6 times larger in the case of PTO. This ratio is almost exactly that of the bulk spontaneous polarization of BTO and PTO.

Electric control of magnetization. So far, we have discussed the magnetoelectric coupling effect in the case of no external bias. A natural question is what happens to ΔM when an external bias V_a is applied. In this case, the electric polarization P will have two parts: the spontaneous polarization P_0 and the induced polarization. The equation determining P is obtained by minimizing the free energy. From the continuity of the normal component of the electric displacement, we find equation relating η and P: $\eta=[(Pt_{FE}/\varepsilon_{FE}) + (V_a/l)]/\{[(\lambda_{FM}+\lambda_{NM})/\varepsilon_0]+(t_{FE}/\varepsilon_B)\}$. Here, ε_{FE} is the dielectric constant of the FE layer. These two equations need to be solved self-consistently. The value of η at a given bias can then be calculated and the induced magnetization ΔM is given by Eq. (4).

The free-energy density F includes contributions from the FE layer, FM layer, and FM/FE interface and takes the form

$$F = \frac{t_{FE}F(P) + t_{FM}F(M) + F_I(P,M)}{t_{FE} + t_{FM} + t_{NM}}. \quad (7)$$

M is the magnetization of the bulk ferromagnet and here $M=M_0$ because of zero external magnetic field. The interface energy $F_I(P,M)$ is the sum of the electrostatic energy and magnetic exchange energy of the screening charges,

$$F_I(P,M) = \frac{(\lambda_{FM}+\lambda_{NM})}{2\varepsilon_0}\eta^2 + \frac{J}{2\mu_B^2}(M+\Delta M)\Delta M. \quad (8)$$

For FE, the free-energy density $F(P)$ can be expressed as $F(P)=F_P+\alpha_P P^2+\beta_P P^4+\int_0^P E_B dP$, where F_P is the free-energy density in the unpolarized state. α_P and β_P are the usual Landau parameters of bulk ferroelectric. E_B is the depolarization field in the FE film. Similarly, $F(M)$ can be expanded as a series in the order parameter M, i.e., $F(M) = F_M+\mu_M M^2+\nu_M M^4$, where F_M is the free-energy density of bulk ferromagnet and μ_M and ν_M are the Landau parameters of bulk ferromagnet. The calculated induced magnetization as a function of the applied bias is shown in Fig. 3. Clearly, the electrically controllable magnetization reversal is realized.

To discuss the macroscopic properties of the electric control of magnetization, we analyze the magnetoelectric cou-

pling energy in our tricomponent superlattice. For the macroscopic average polarization to be represented by the electric polarization obtained for a unit cell, this cell needs to be chosen with special care.[25] Therefore, in the following calculation of total free energy, unit cell B in Fig. 1(b) is chosen, and

$$\bar{P} = \frac{P t_{FE} + \eta(t_{FM} + t_{NM})}{t_{FE} + t_{FM} + t_{NM}}. \quad (9)$$

The macroscopic average magnetization $\bar{M}$ is

$$\bar{M} = \frac{M t_{FM} + \Delta M}{t_{FE} + t_{FM} + t_{NM}}. \quad (10)$$

Considering the lowest-order term of the magnetoelectric coupling, $\bar{P}$ and $\bar{M}$ can be expanded as $\bar{P} = c_p P + c_p' P M^2$, $\bar{M} = c_m M + c_m' P M$. Therefore, the total free energy [Eq. (7)] can be expressed as the power series of $\bar{P}$ and $\bar{M}$, $F(\bar{P},\bar{M}) = F_0 + \alpha \bar{P}^2 + \beta \bar{P}^4 + \mu \bar{M}^2 + \nu \bar{M}^4 + \chi \bar{P} \bar{M}^2 + \cdots$. We would like to point out that biquadratic ME coupling $\bar{P}^2 \bar{M}^2$ is easily achievable, but is usually weak and is not electrically controllable. However, because of the naturally broken inversion symmetry, the large ME coupling $\bar{P} \bar{M}^2$ is possible in our tricomponent structure.

The ME coupling in FM/FE/NM superlattices may be observed experimentally and may have practical applications. Although the net additional magnetization of each FM/FE/NM unit cell is small, stacking several of them in a superlattice will result in a large overall magnetization. From Eq. (10), with a thinner metallic electrode, the ME effect will be larger, as long as the thicknesses of metallic electrodes are larger than the screening length, which is easy to achieve.

To summarize, expanding upon the theory of spin-dependent screening,[12] we develop a theory of additional magnetization in tricomponent superlattice. We show that the additional magnetization can be electrically controlled and is linear in FE polarization. The latter can be switched if the coercive voltage of the ferroelectric is reached. We demonstrate that an asymmetric FM/FE/NM structure has practical advantages over the previously discussed symmetric structure.

T.C. and Q.N. were supported by DOE (Contract No. DE-FG03-02ER45985), NSF (Contract No. DMR0906025), Welch Foundation (Contract No. F-1255), and NSFC (Contract No. 10740420252). T.C. was supported by K. C. Wong Education Foundation, Hong Kong and China Postdoctoral Science Foundation. J.L., N.S., and A.A.D. were supported by the Office of Naval Research (Contract No. N000 14-06-1-0362) and Texas Advance Computing Center.

[1] M. Fiebig, J. Phys. D **38**, R123 (2005).
[2] N. A. Hill, J. Phys. Chem. **104**, 6694 (2000).
[3] W. Eerenstein, N. D. Mathur, and J. F. Scott, Nature (London) **442**, 759 (2006).
[4] S.-W. Cheong and M. Mostovoy, Nature Mater. **6**, 13 (2007).
[5] R. Ramesh and N. A. Spaldin, Nature Mater. **6**, 21 (2007).
[6] Y. Tokura, J. Magn. Magn. Mater. **310**, 1145 (2007).
[7] A. Malashevich and D. Vanderbilt, Phys. Rev. Lett. **101**, 037210 (2008).
[8] C. J. Fennie and K. M. Rabe, Phys. Rev. Lett. **97**, 267602 (2006).
[9] H. Zheng, J. Wang, S. E. Lofland, Z. Ma, L. Mohaddes-Ardabili, T. Zhao, L. Salamanca-Riba, S. R. Shinde, S. B. Ogale, F. Bai, D. Viehland, Y. Jia, D. G. Schlom, M. Wuttig, A. Roytburd, and R. Ramesh, Science **303**, 661 (2004).
[10] F. Zavaliche, T. Zhao, H. Zheng, F. Straub, M. P. Cruz, P.-L. Yang, D. Hao, and R. Ramesh, Nano Lett. **5**, 1793 (2005).
[11] C. G. Duan, S. S. Jaswal, and E. Y. Tsymbal, Phys. Rev. Lett. **97**, 047201 (2006).
[12] S. F. Zhang, Phys. Rev. Lett. **83**, 640 (1999).
[13] J. M. Rondinelli, M. Stengel, and N. A. Spaldin, Nat. Nanotechnol. **3**, 46 (2008).
[14] C.-G. Duan, J. P. Velev, R. F. Sabirianov, Z. Zhu, J. Chu, S. S. Jaswal, and E. Y. Tsymbal, Phys. Rev. Lett. **101**, 137201 (2008).
[15] T. Maruyama, Y. Shiota, T. Nozaki, K. Ohta, N. Toda, M. Mizuguchi, A. A. Tulapurkar, T. Shinjo, M. Shiraishi, S. Mizukami, Y. Ando, and Y. Suzuki, Nat. Nanotechnol. **4**, 158 (2009).
[16] P. Batra and B. B. Silverman, Solid State Commun. **11**, 291 (1972); P. Wurfel and I. P. Batra, Ferroelectrics **12**, 55 (1976).
[17] J. Junquera and P. Ghosez, Nature (London) **422**, 506 (2003).
[18] N. Sai, A. M. Kolpak, and A. M. Rappe, Phys. Rev. B **72**, 020101(R) (2005).
[19] E. Y. Tsymbal and H. Kohlstedt, Science **313**, 181 (2006).
[20] M. Ye. Zhuravlev, R. F. Sabirianov, S. S. Jaswal, and E. Y. Tsymbal, Phys. Rev. Lett. **94**, 246802 (2005).
[21] S. Ju, T. Y. Cai, G. Y. Guo, and Z. Y. Li, Phys. Rev. B **75**, 064419 (2007).
[22] A. M. Bratkovsky, Phys. Rev. B **56**, 2344 (1997).
[23] J. K. Lee, N. Sai, T. Y. Cai, Q. Niu, and A. A. Demkov (unpublished).
[24] The DFT calculations were performed within the local spin-density approximation as implemented in VASP; G. Kresse and J. Furthmüller, Phys. Rev. B **54**, 11169 (1996). We have used a plane-wave energy cutoff of 600 eV and a $6\times6\times1$ Γ centered k-point mesh for the integration of the Brillouin zone.
[25] The polarization (i.e. computed via the Berry phase) is of course cell independent. There is, however, one "natural" cell for which the macroscopic average polarization can be represented by the cell dipole. That fact is used in Eq. (9) and unit cell B is chosen. In one-dimensional case, assuming that electric current J is a nonspinor and choosing an appropriate gauge, the fundamental laws of electrodynamics are $\frac{dP}{dx} = -\rho$ and $J = \frac{\partial P}{\partial t}$. Here, P is the electric polarization and ρ is the charge density. Choosing an appropriate unit cell, the macroscopic average polarization can be represented by the cell dipole, i.e., $\int_{x_1}^{x_2} \dot{P} dx = \int_{x_1}^{x_2} \dot{\rho}(x) dx$, where x_1 and x_2 are the boundaries of the unit cell. Combing this with $\frac{dP}{dx} = -\rho$ and $J = \frac{\partial P}{\partial t}$, it is found that its left-hand side is $\int_{x_1}^{x_2} J dx$, while its right-hand side is the sum of $-J(x)x\big|_{x_1}^{x_2}$ and $\int_{x_1}^{x_2} J dx$. Thus, only when the condition of no charge exchange between the neighboring unit cells is satisfied, i.e., $J(x_1) = J(x_2) = 0$, the macroscopic average electric polarization can be represented by the cell dipole. Unit cell A is not the appropriate one because the current will develop across it during polarization switching.